Experimental and numerical assessment of grain boundary energies in polycrystalline uranium dioxide

A. Ksibi, X. Iltis, E. Bourasseau, D. Drouan, M. Gaudet, A. Germain, Alexandra Pena Revellez, G. Lapertot, J.-P. Brison, R.C. Belin

Experimental and numerical assessment of grain boundaries energy in polycrystalline uranium dioxide

A. Ksibi[1], X. Iltis[1], E. Bourasseau[1], D. Drouan[1], M. Gaudet[1], A. Germain [1], A. Pena[3], G. Lapertot[2], J.-P. Brison[2] and R. C. Belin[1*]

[1] CEA, DEN/DEC, Cadarache, 13108 St Paul Lez Durance, France

[2] University Grenoble Alpes, CEA, IRIG-PHELIQS, F-38000 Grenoble, France

[3] Univ. Grenoble Alpes, CNRS, Grenoble INP, Institut Néel, 38000 Grenoble, France

* Corresponding author: renaud.belin@cea.fr

***Abstract*:**

Uranium dioxide ceramics are widely used as nuclear fuels. Thus, it is important to understand the role of the grain boundaries (GBs) which decisively govern the properties of these polycrystalline materials and subsequently determine their performances. Here, we report a coupled numerical - experimental approach enabling to assess GB energies. Firstly, GB formation energies (γ_{gb}) were computed for 34 symmetric tilt GBs in UO_2 with molecular dynamics simulations at 1700 K. The surface energies (γ_S) relative to the respective planes of these GBs were calculated as well. The Herring relation was then used to assess the dihedral angles Ψ of the corresponding GB grooves. Secondly, a UO_2 ceramic sample was annealed at 1673 K to obtain GB grooves. The CSL GBs of interest were identified by EBSD and their Ψ angles determined by AFM. Computed and measured Ψ values were found to be very close.

Keywords: Uranium dioxide, UO_2, Grain boundaries, Groove, Thermal grooving theory, Grain boundary energy, surface energy, CRG potential

I. Introduction

Polycrystalline uranium dioxide (UO_2) has received a thorough attention owing to its extensive use as fuel in the current nuclear pressurized water reactors (PWRs). This oxide is elaborated in the form of refractory ceramics composed of grains, with a size of about ten microns, by means of a powder metallurgy process [1]. The grains bond together by internal interfaces known as grain boundaries (GBs). Such GBs are a key element of the microstructure, decisively influencing the macroscopic properties that determine the material performances. In nuclear fuels, the GBs can be subjected to an intergranular decohesion under the effects of irradiation, as a consequence of thermomechanical stresses derived from the temperature gradient and the accumulation of fission gas bubbles. Thus, a detailed description of GBs in UO_2 and a determination of their characteristics, in particular of formation energies and/or mechanical properties (toughness, strength, etc.), are highly required to better understand the role of GBs in governing the UO_2 fuels properties.

A GB is seen as being one of the planar defects in material microstructure and possesses complex crystallographic features. To well describe a GB, five independent parameters, better known as macroscopic Degrees Of Freedom (DOFs), are involved [2]. While three of them determine the crystallographic elements that typify the relationship between two adjacent grains (the axis *[uvw]* and the angle of misorientation θ), the two other parameters specify the orientation of the boundary of one of the grains and define the GB plane *(hkl)*.

These crystallographic characteristics allow to describe a GB using the following notation: $\sum n$ *(hkl) / [uvw]-*θ, and, particularly, influences the energy of the GB (γ_{gb}) which does strongly depend on its crystallographic structure [3]. Many experimental studies have effectively reported the crystallographic characteristic dependence of γ_{gb} within polycrystalline systems [4–7]. Such energy, which represents the excess free energy per unit area due to the presence of the boundary with reference to the perfect crystal, has been the subject of a great deal of research for many decades. Indeed, Read and Shockley [8] suggested the first model enabling to determine γ_{gb}. However, this model, based on a hypothesis considering the GBs as dislocation defects, is limited exclusively to GBs having small misorientation angles θ ($\theta \leq 15°$). Subsequently, Herring [9] reported the theory of thermal grooving which has become one of the common methods for experimentally probing γ_{gb}. It consists in measuring the geometry of the grooves revealed by a thermal etching where the boundaries intersect a free surface (Figure 1). The grooves, formed to reduce the total surface free energy of the system, are described as the result of a local equilibrium

between the boundary and the solid-vapor interface. This equilibrium is expressed by Herring equation [9,10]:

$$\gamma_{gb} = 2\,\gamma_S \cos\left(\frac{\psi}{2}\right) - 2\,\frac{\partial \gamma S}{\partial \psi} \sin\frac{\psi}{2} \qquad \textit{equation 1}$$

where γ_{gb}, γ_s and Ψ are the GB energy, the surface energy of the crystal and the surface dihedral angle, respectively.

Moreover, Mullins [10] successfully used a bundle of simplifications to ease the determination of the GB energy by adopting suitable boundary conditions as follows:

- The system is closed and the polycrystalline material in quasi-equilibrium with its vapor.

- The matter transport occurs only by surface self-diffusion.

- The surface energy does not depend on the crystallographic orientation, then γ_s is isotropic and its anisotropy can stem exclusively from faceted surfaces.

- The GB is perpendicular to the crystal surface.

Thus, the Herring relation [9] can be simplified as:

$$\gamma_{gb} = 2\,\gamma_S \cos\frac{\psi}{2} \qquad \textit{equation 2}$$

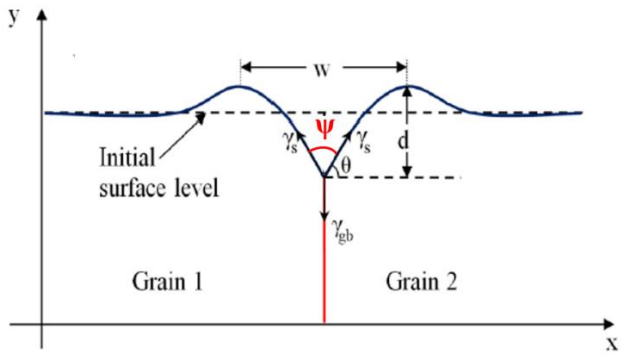

Figure 1: Schematic illustration of the force balance in a boundary intersecting a free surface.

Yet, the experimental GB energy remains difficult to measure, as exemplified by the scattering in the published values that are furthermore available only for a few particular GBs in a given material. Most of such γ_{gb} energy data, on the other hand, were reported for metals and, to lesser extent, for ceramics [4,7,11–17]. Indeed, most reports focused on the assessment of the relative energy (γ_{gb}/γ_s) without reporting the γ_{gb} [18–20] because the choice of the energy surface γ_S is crucial. For example, Kelly *et al.* [21] used the thermal grooving method to measure the

dimensions of GB grooves on the surfaces of a polycrystalline alumina, and then estimated γ_{gb}/γ_s at different temperatures. They reported a mean value $\gamma_{gb}/\gamma_s = 1$ at 1673 K which is similar to those reported by Handwerker *et al.* [17] ($\gamma_{gb}/\gamma_s = 1.2$), Saylor *et al.* [22] ($\gamma_{gb}/\gamma_s = 1.2$) and Dillon *et al.* [23] ($\gamma_{gb}/\gamma_s = 1.11$) at the same temperature using different methods. To the best of our knowledge, GBs energies have never been experimentally determined for UO_2.

Nonetheless, it is quite usual for authors to assume that γs is isotropic and corresponds to a specific value. Here it is important to note that the term « isotropic » is ambiguous. Usually, one considers that a property will be isotropic if it is independent of the crystallographic orientation. Yet, it is not clear whether or not this is true throughout the entire sample or if it is only true at the vicinity of a given GB groove. As an example, Shibata *et al*. [19] evaluated the absolute γ_{gb} of nine types of symmetric tilt GBs possessing the same rotation axis [110] in an yttrium-stabilized cubic zirconia bicristal by using an average γ_s value of 1.21 $J.m^{-2}$. Note that similar studies were published later by Yoshida *et al.* [18]. It is worth noting that the reported γ_s is a unique value obtained by an approximation that may not allow a realistic vision of a complex polycrystalline material, as will be discussed in §II.1.

It is therefore clear that the experimental determination of γ_{gb} is challenging and that numerical simulations can be an alternative approach to assess this property. Such methods have been successfully employed for studying GBs, opening up the possibilities for a deeper understanding of the crystallographic GB structure. However, very few works, addressing the GB energy particularly in UO_2, have been published so far. Note that these studies have been recently reviewed [25]. In the latter, extensive molecular dynamic simulations of 26 tilt CSL GBs are reported and their formation energies at 300 K calculated using four different empirical potentials.

In the present work, molecular dynamics simulations were first employed to compute the surface energies γ_s and the formation energies γ_{gb} of 34 symmetric tilt GBs using the CRG potential at 1700 K. The obtained computational data allowed to highlight that the Mullins conditions are fulfilled with respect to a certain way of considering the isotropy of γ_s. The dihedral angle ψ values were hence estimated from the Herring equation.

Then, special GBs were identified by Electron BackScatter Diffraction (EBSD) on a mirror-polished UO_2 ceramic sample that first underwent a thermal etching to obtain GB grooves. Atomic Force Microscopy (AFM) was thereafter used to experimentally assess the dihedral angles ψ of selected GBs. Experimental and calculated ψ angles were finally compared and discussed.

II. Calculation results

1. Methodology

The GB energy in UO_2 was assessed by means of simulations at the atomic scale GBs were built using GBStudio software [26], based on their CSL classification and the crystallographic structure of the examined material. The GB construction was performed in purely geometrical terms from two crystals for which the respective directions were chosen to meet the macroscopic DOF of the targeted GB (orientation of the two crystals and GB plane). The relative position of the crystals with respect to each other, as well as the position of the atoms at the interface, were then relaxed with the aim of reducing the energy of the system, and then assessing the energy of the targeted GB. The relaxation procedure was applied as follows [25]:

- Firstly, the energy was minimized at 0 K, enabling the relaxation of the simulation box (Figure 2) and the positions of the atoms, thereby inducing a stable configuration suitable for simulating the system dynamics at a given temperature.
- Secondly, a thermal annealing was applied using the molecular dynamic code LAMMPS [27]. The temperature was increased in 1 ns from 0 to 1870 K, and maintained for 0.4 ns, assuming potential energetic barriers could easily be overcame at such a temperature level. The temperature was then decreased to 1700 K in 1 ns, and the calculation of energy and volume averages was performed at this temperature value during 4 ns.

The GB energy is the excess energy resulting from the presence of an interface compared to the energy of the corresponding single crystal. Hence, this energy can be calculated using the following formula:

$$E_{gb} = \frac{e^N_{Bicristal} - e^N_{Monocristal}}{2A} \qquad \textit{equation 3}$$

Where $e^N_{Bicristal}$is the energy of a system of N atoms including explicitly the GB, $e^N_{Monocristal}$ the energy of a single crystal with the same number of atoms calculated in the same conditions. A is the surface of the simulated boundary, *i.e.* the section of the simulation box (cf. Figure 2).

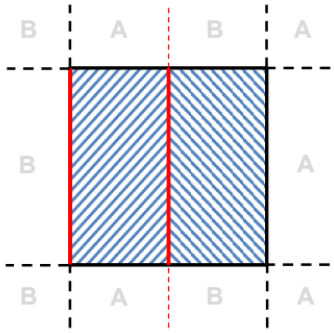

Figure 2: Schematic of the simulated system with a GB. The simulation box, in the center, contains two crystals A and B.

It should be noted that our simulations were carried out with periodic boundary conditions to prevent free surface effects. Consequently, two similar GBs are simulated, explaining the factor 2 in the denominator of the *equation 3*. The energy calculated with *equation 3* is not related to the solidity of the GB but rather expresses its thermodynamic stability, compared to the single crystal. The larger is the GB energy, the more unstable is the GB in a thermodynamic perspective.

In this study, we also calculated surface energies (γs) for the GB planes of all the considered symmetric tilt GBs, following the same procedure as for GB energy and at the same temperature. It finally consists in performing the relaxation of the half of the system represented in Figure 2. For a given CSL GB, the GB plane is the first and generally the most favorable one proposed by GBStudio.

We used the CRG potential from Cooper *et al.* [26] to calculate both the GB and surface energies. This potential enables an approximate but proper description of the interactions between atoms, required for an efficient calculation of the forces acting on the latter, and subsequently for an assessment of the system energy. In fact, the most common GBs observed in the UO_2 polycrystalline material were previously simulated at 300 K using four empirical potentials with the procedure of construction and relaxation of special GBs [25]. As a result of this study, the CRG potential was selected to assess the GB energy mainly for two reasons:

i) The energies calculated using this potential at 300 K were consistent with the classification of the GBs as a function of the linear fraction measured by EBSD [25].

ii) This potential yielded good results with regard to the evolution of thermodynamic properties with temperature [28].

2. Surface energy

The surface energy is one of the fundamental properties, very sought after for understanding the phenomena occurring at the GBs. Different techniques are available to experimentally determine γs in polycrystalline ceramics [29], but they are complex and the measured γs appears to depend on the used technique. Indeed, many research groups reported on γs measurements in polycrystalline [30–33] and pointed out the difficulty of assessing γs, evidencing the scattering in the experimental γs values.

Thus, in the present work, the γs property was rather calculated using atomistic simulations for different crystallographic planes. Various studies reported calculated low indexes γs (111), (110), and (100) in UO_2 by using semi-empirical methods or ab-initio calculations [34–37]. Recently, Bourasseau *et al*. [25] computed γs for the same three crystallographic planes and compared the obtained results with data from other authors.

Figure 3 depicts the γ_s values computed for the planes of 34 symmetric tilt GBs which are described by their respective crystallographic notations on the x-axis. GBs possessing the same rotation axis are evidenced with the same color, and ranked by increasing misorientation angles. With the notable exception of the axis [110], we observe that the planes of GBs possessing the same rotation axis display relatively similar γs with a difference between values that does not exceed 0,2 $J.m^2$. A slight evolution of the gamma as a function of the disorientation angle is visible, increasing or decreasing depending on the axis, confirming that γs in UO_2 polycrystalline material depends on the crystallographic orientation of the surface, as reported in the literature. Concerning the axis [110], it is less obvious to make the same observation, but we can however distinguish two groups of GBs having consistent γ_s values (around 1.27 $J.m^{-2}$ for 5 GBs and around 1.73 $J.m^{-2}$ for 3 GBs). Finally, in spite of the dependence of γ_s with the crystallographic orientation of the surface, we show here that it is a reasonable hypothesis to consider that the γ_s value is identical for the planes of GBs with the same rotation axis. We note however that [110] GBs exhibit two distinct values, on the one hand, and that only a single γs value is provided for each of the [321], [331] and [551] axis, on the other hand.

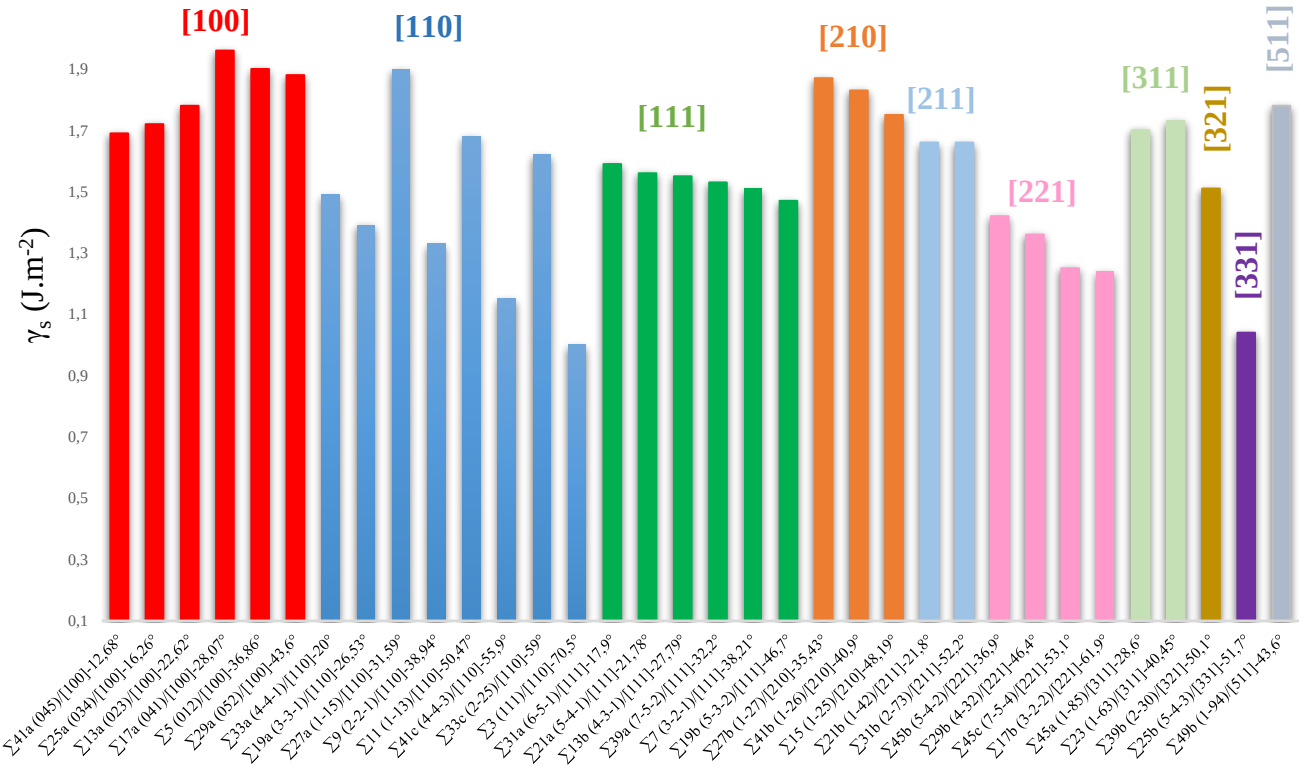

Figure 3: Surface energies of the GB planes of 34 symmetric tilt GBs (J.m^{-2}). The GBs possessing the same rotation axis are represented with the same color.

3. *Formation energy of symmetric tilt grain boundaries*

Herein, γ_{gb} of a batch of 34 symmetric tilt GBs, with different misorientations and a range of different boundary plane orientations, have been computed at the temperature of 1700 K using the CRG potential.

Figure 4 depicts the γ_{gb} values calculated using *equation 3* for these GBs described by their respective crystallographic notations on the x-axis. The γ_{gb} values are within the range 1.2 – 2.11 J.m^{-2} with an error bar of 0.05 J.m^{-2}. This error originates from the empirical choices for the minimization process as well as from the statistical uncertainty tied to molecular dynamics. We note, in particular, that γ_{gb} at 1700 K were slightly enhanced compared to those reported at 300 K, with an increase in between 0,08 J.m-^{2} obtained for ∑11 and 0,3 J.m-^{2} for ∑3.

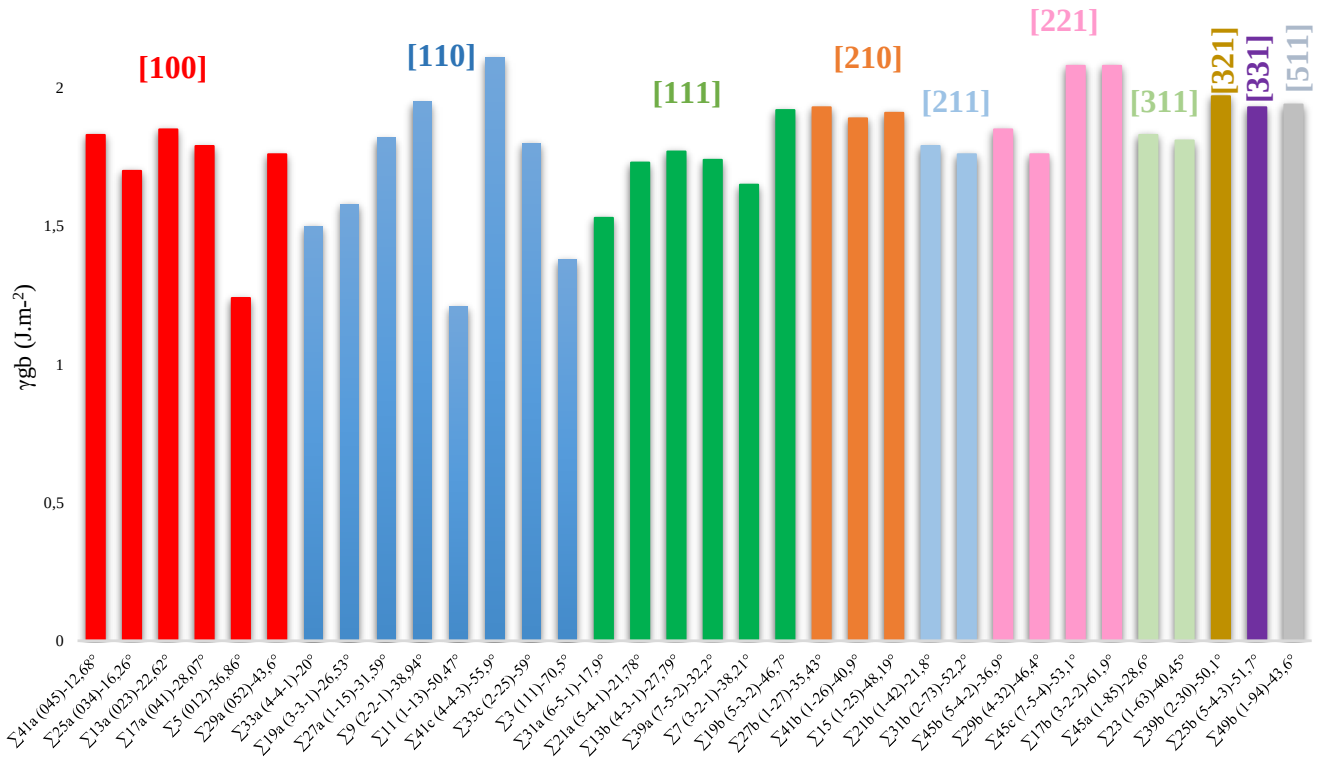

Figure 4: GB energies of 34 symmetric tilt GBs at 1700K (J.m^{-2}).

Figure 5 exhibits γ_{gb} as a function of misorientation angle θ, for the [100], [110] and [111] symmetric tilt GBs, respectively. For better clarity, ∑ indices are indicated as well. By increasing θ, the energy magnitude fluctuates more for [110] GB than for [100] and [111] GBs, and no obvious correlation exists between γ_{gb} and θ. This confirms that the parameter θ only is not sufficient to determine γ_{gb}.

Looking at the energy cusps evidenced on the curves, the lowest γ_{gb} values can be easily obtained. Indeed, in [110] GBs (red points in Figure 5), we distinct two energy cusps at ∑3 with the boundary plane of (111) and ∑11 with (113), and the latter displays the lowest γ_{gb} (~1.2 J.m^{-2}). We note also that, among all the investigated GBs, ∑41c boundary shows the largest γ_{gb} value. Therefore, γ_{gb} could not be correlated only to the ∑ value. In the [100] GBs (blue dots), the ∑5 and ∑25a GBs display energy cusps, with the lowest γ_{gb} for the ∑5 one, which is in coherence with its highest linear fraction. Regarding the [111] GBs (green squares), we notice only single cusps at ∑7 that present larger γ_{gb} compared to those mentioned above.

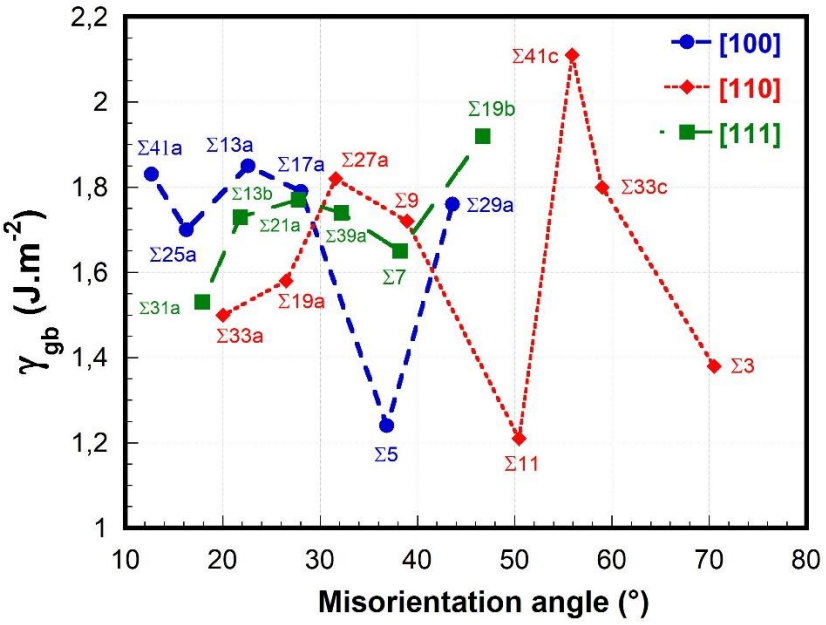

Figure 5: GB energy as a function of misorientation θ for [100], [110] and [111] symmetric tilt GBs at 1700 K.

III. Experimental grain boundary energy measurements

1. Methodology

1.1 Sample preparation and characterization

A 16 mm – thick and 8 mm – diameter pellet was elaborated using a UO_2 powder metallurgy process in the UO_2 Laboratory at CEA – Cadarache, France. The powder was uniaxially cold-pressed under 400 MPa and then sintered at 1950 K for 4 h under Ar + 5% H_2 atmosphere to ensure the material stoichiometry. A 1.5 mm thick disc was thereafter cut from the central part of the pellet and underwent a mechanical polishing with a final step performed with a 0.02 µm colloidal silica suspension to minimize the polishing superficial impact.

Furthermore, six Vickers micro-indents were performed using an Anton Paar MHT-10 micro-indentation instrument on the polished surface of the samples to mark a region of interest of 1024 µm x 704 µm, containing about 850 grains, with the aim of easily locating it before and after characterization by EBSD.

In order to create GB thermal grooves, the polished specimen was placed in a furnace and heated up to 1673 K, then was maintained for 4 h, under Ar + 5% H_2 atmosphere before being cooled down at 5 K/min. The applied annealing conditions were selected not only to achieve well-grooved GBs, but also to avoid significant grain growth and to preserve the material stoichiometry.

To select the type of GBs, EBSD analyses were performed on the region of interest identified above using a FEI NovaNano SEM 450, equipped with a Nordlys II Nano camera (maximum CCD resolution: 1344 × 1024 pixels) and the process-driven software AZTEC (from Oxford Instruments). EBSD data were acquired with a camera binning set to 4×4, a step size of 0.4 µm, an acceleration voltage of 20 kV, a beam current of about 10 nA, and a working distance of 15 mm. They were then analyzed with the Channel 5 suite of programs. The indexation rate of EBSD data (ratio of indexed pixels over total number of tested pixels) was close to 98% (prior to any data cleaning).

1.2 Dihedral angle evaluation

Grain boundary energies for the present sample were estimated from dihedral angle on thermally grooved surface. AFM was used with the aim of measuring the key parameters typifying the groove geometry formed at the boundaries. Images were recorded using a NSV-VEECO-D3100 AFM operating in tapping mode. AFM data processing was performed using Gwyddion software [38], which enabled to extract the cross-sectional profile of the groove along a line taken perpendicular to a GB, as illustrated in Figure 1. For each profile, the width

(W) and depth (d) were directly measured and the ψ value was calculated using the Mullins theory and the following equation [39]:

$$\Psi = 180 - 2\tan^{-1}(4.73 \times (\frac{d}{w/2})) \qquad \textit{equation 4}$$

Note that ten measurements were performed on each GB in view of checking the degree of reproducibility.

2. Surface energy anisotropy

As previously mentioned, the most significant simplification made in the Mullins model is the assumption of the full isotropy of γ_s. Obviously, in UO_2, γ_s varies substantially with crystallographic orientation like in most materials. This energy variation creates anisotropy in γ_s, which leads to the formation of surface faceting features during annealing. Surface faceting is correlated with the crystallographic orientation of the grain. The formation of ridges was observed in the surface grains on different materials [40–46].

Figure 6a shows SEM micrographs, acquired in Back-Scattered Electrons (BSE) mode, of the polished surface of the UO_2 polycrystalline sample after the annealing treatment. It can be clearly seen that the GBs are well grooved, and that the surfaces of some grains exhibit ridges. The formation of ridges on the grain surface as indicated by arrows on figure 6a clearly reveals an anisotropy of γ_s for some grains. EBSD analysis tends to reveal that ridges would form preferentially on surfaces with crystallographic orientations relatively close to (001): see Figure 6b, on which grains presenting marked ridges were selected manually on the EBSD map by comparing it with the electronic image given by the Forward Scatter Detectors (FSD) mounted on the EBSD camera. Matzke [43] observed also this phenomenon in annealed UO_2 polycrystalline sample. Later, such a phenomenon was studied by Miao *et al.* [47] in UO_2, in order to establish a correlation between the crystallographic orientation and faceting features of polycrystalline UO_2 using Synchrotron and Laue microdiffraction. These authors studied the change in surface morphology for all stereographic triangle directions. They concluded that triple-plane structures containing one (100) plane and two (111) planes with three <110> edges dominated in most cases the surface morphology of UO_2. The dominance of this structure can be explained by the stability of low-energy surfaces.

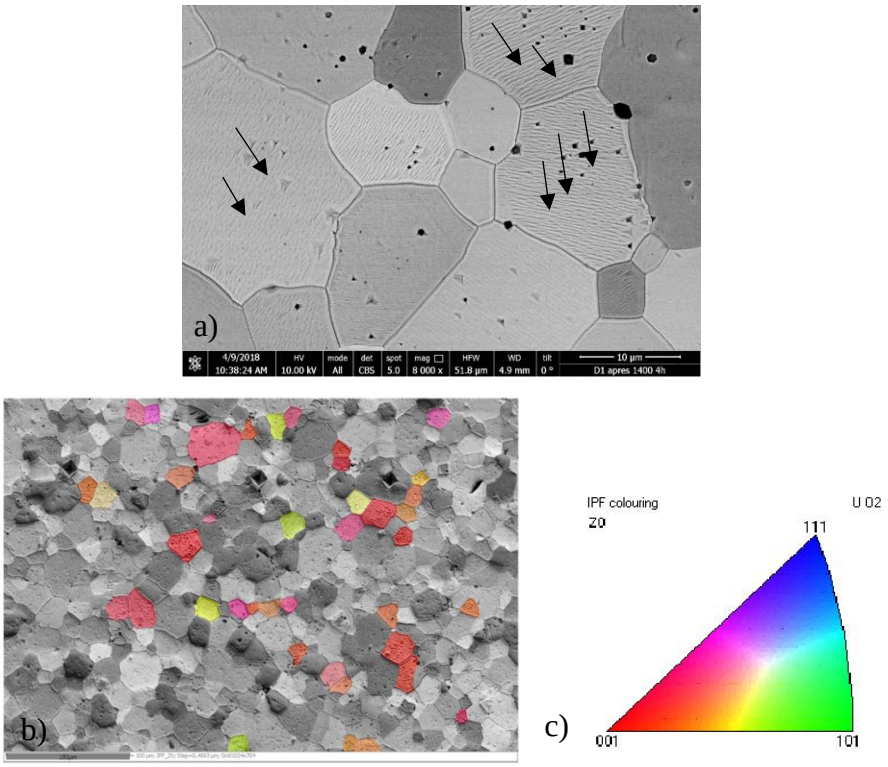

Figure 6: a) SEM micrographs (in BSE mode) of the annealed UO_2 specimen revealing GB grooves and some grains with ridged surfaces (black arrows indicate some ridges), b) FSD electron image superimposed with EBSD map grains exhibiting marked ridges were selected manually and are colored according to the IPF-Z color code given in (c).

3. Experimentally observed thermal grooves

It is reported that the surface anisotropy may strongly affect the GB groove morphology and, thereby causes the formation of facets instead of a smoothed boundary groove [48]. The presence of such facets prevents from determining the dihedral angle of the groove and applying Mullins theory.

In the present study, CSL boundaries identified by EBSD mapping were investigated using the AFM technique. Typical AFM micrographs of the GB grooves in the polycrystalline UO_2 specimen annealed at 1673 K for 4h, with the corresponding line topographic profiles, are given in Figure 8.

A set of GBs was examined in detail. Their GB groove profiles revealed different morphologies, which can be gathered in two categories: symmetric and asymmetric.

A symmetric groove is illustrated in Figure 8a, which shows a profile with two symmetrical humps presenting the typical morphology defined by Mullins [10].

Asymmetric GBs can be either unfaceted or faceted. The vast majority of the GB groove profiles showed a significant groove asymmetry that is clearly different from the classical profile predicted by Mullins theory but is consistent with studies previously reported on ceramics oxides [17, 50–52].

Figure 8b depicts a faceted groove while Figure 8c shows a smooth groove profile with asymmetric humps. Both grooves might result from either the inclination of the GB plane or the surface anisotropy (γs) of the grain.

i) Inclined GB plane

As stipulated by Mullins, if the GB plane is perpendicular to the material free surface then the angle α between the GB and the direction normal to the specimen is zero as illustrated in Figure 7a. Nevertheless, not all GB planes in a polycrystalline material can be orientated normal to its free surface. They can be inclined (Figure 7b) which means that the angle α can be different from zero, as noted by Shin *et al.* [50] in thermally etched alumina.

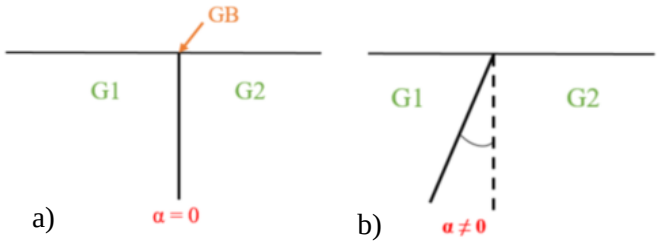

Figure 7: A schematic showing the GB plane a) perpendicular (α = 0), and b) inclined (α ≠ 0) to the material free surface.

ii) Surface energy anisotropy γ_S and faceting

Several authors in the literature addressed the effect of surface anisotropy on the morphology of GB grooves [44,45,52–56]. Rabkin et *al.* [54] observed unusual GB groove morphologies using AFM on the NiAl surface after annealing at 1400°C. They attributed the asymmetry they found for GB grooves to the presence of a vicinal surface on one side of a groove and modified Mullins' [10] linearized equation for thermal GB grooving to take the negligible mass transport on the vicinal surface into account.

Sachenko *et al.* [45] showed that a groove developed between faceted and unfaceted (smooth) grains is often asymmetric with unusual growth kinetics. They explained the groove asymmetry by surface diffusion anisotropy, considering that the diffusion coefficient is high on the unfaceted side while it is negligible on the faceted side of the groove.

Zhang *et al.* [44] studied the effect of anisotropic surface free energy on thermal GB grooving using modeling, simulation and experiments on tungsten. Based on Herring's model, they

showed that, when the anisotropy is mild, the groove profiles are self-similar in the evolution but are often not in proportion to those developed under isotropic material properties. When the anisotropy is critical, surface faceting occurs. In addition, when it is severe the facets coarsen in the evolution. They exhibit the groove profiles in evolution under different degrees of anisotropy.

To the best of our knowledge, the GB groove morphology has never been experimentally studied for UO_2.

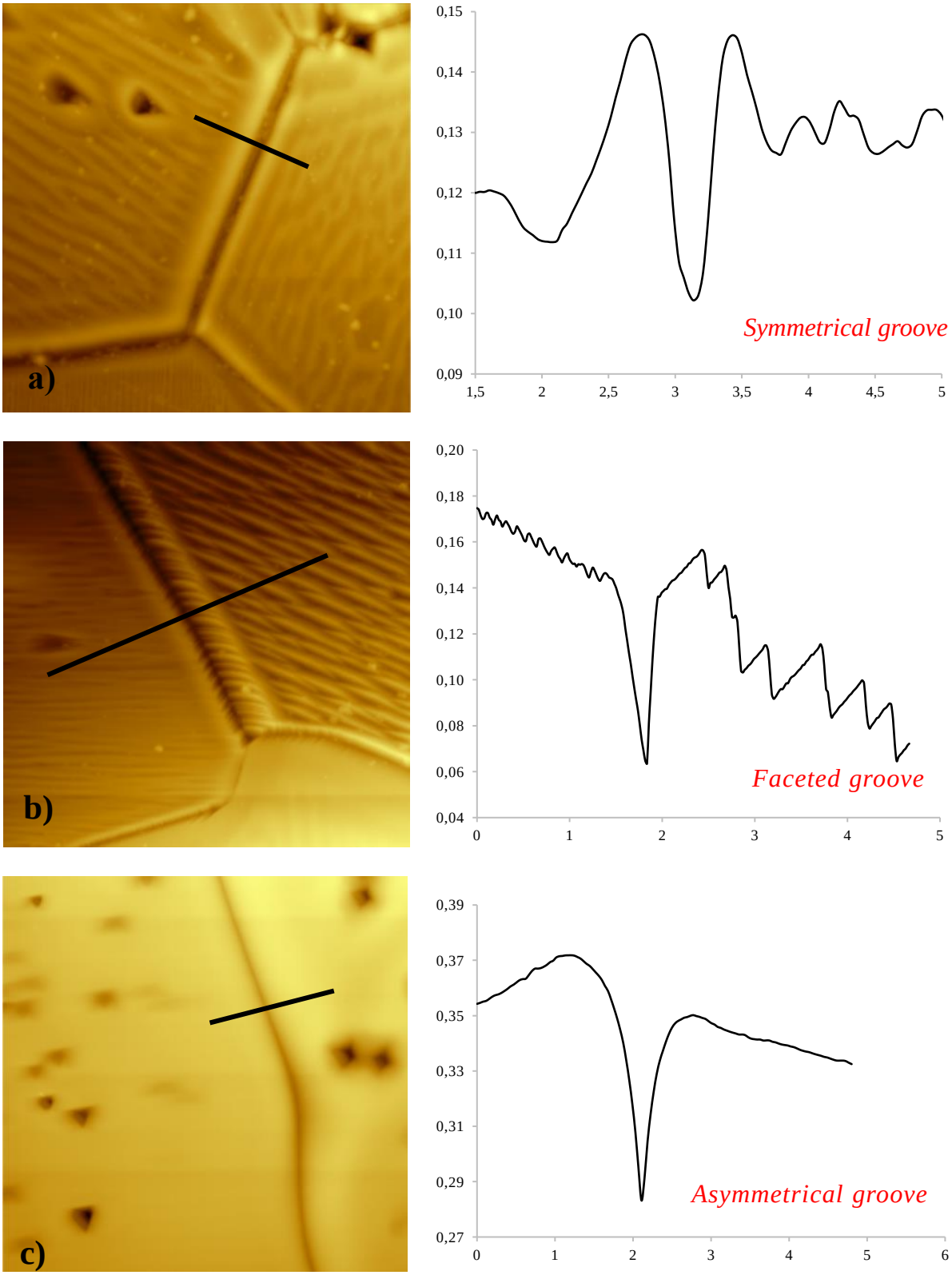

Figure 8: AFM images of GB grooves in the UO2 sample annealed at 1673 K for 4h, and selected linear profiles taken perpendicular to the GB direction. a) Symmetrical groove, b) asymmetrical faceted groove and c) asymmetrical unfaceted groove.

4. Dihedral angle ψ measurement

EBSD measurements were first used to identify the GB character in the region of interest of the annealed specimen, thereby selecting special CSL GBs for which ∑ values up to 49 (as classically considered for cubic crystals) were assigned. Grain boundaries with misorientations greater than 5° degrees were taken into account. The total linear fraction of CSL boundaries attains 14.56%, which is very close to the values reported by Nerikar *et al.* [57] (15.7%) and in our previous work (14.9%) [25] for UO_2 ceramics.

Secondly, experimental measurements of a dihedral angle ψ were performed for the above-identified CSL GBs solely from the profile of symmetrical grooves of GBs. With this criterion, 25 GBs were exploitable in the region of interest.

The ψ values, obtained for the CSL GBs in the specimen annealed at 1673 K, are tabulated with their macroscopic parameters in Table 1. For each GB, the ψ value is the average of at least ten measured values, the difference between the minimum and the maximum ones being within the range 2° to 10°. It must be noted that the measurements were made on a polycrystalline specimen, which means that the tilt or twist character and the nature of the plane of a given GB cannot be determined.

CSL Index	***Axis***	***Misorientation angle (°)***	***Measured ψ angle (°)***
∑3	110	70,5	93
∑5	100	36,86	138
∑7	111	38,21	111
∑9	110	38,94	78
∑13b	111	27,79	109
∑15	210	48,19	110
∑19a	100	28,07	109
∑21a	111	21,78	112
∑21b	100	16,26	94
∑23	311	40,45	115
∑25b	331	51,7	125
∑29b	221	46,4	83
∑33a	110	20	136
∑39a	111	32,2	115
∑41a	100	12,68	126
∑45b	221	36,9	104
∑49b	511	34,6	113

Table 1: ψ measured on AFM linear profiles of the grooves etched on the identified CSL GBs.

IV. Comparison of experimental and atomistic simulations relative energies

To be able to compare experimental and atomistic simulations results, a relationship between experimental dihedral angles and calculated energies can be found by applying the Herring equation in a reverse fashion. Thus, we consider here a "virtual" thermal etching on simulated GBs involving virtual GB grooves and dihedral angles as represented in Figure 1. In those conditions, the rotation axis of simulated GBs is included in their respective GB planes and parallel to the virtual surface of the sample. As already noted, γ_s values calculated for all the planes boundaries of the GBs possessing the same rotation axis are nearly similar, we can therefore consider that, for a given rotation axis, γ_s is identical to the surface energy of the GB plane at the root of the virtual groove of the GB. In other words, for a given rotation axis, we can consider that the derivative of γ_s in regard of ψ is negligible. This standpoint allows using the simplified Herring equation to determine the corresponding virtual calculated dihedral angles from the calculated values of γ_s and γ_{gb}. Note that when discussing γ_s at the groove of GB, we will then use the word « identical » instead of isotropic, as it is now clear that γ_s is not isotropic throughout the sample (cf. section III.2).

Figure 9 compares the experimental and calculated dihedral angles ψ for 11 GBs. The calculated and measured ψ show a good agreement. In general, boundaries with higher measured angle ψ have higher calculated angle ψ. The relative difference between calculated and experimental values is under 5 %, except for Σ3, Σ21b, Σ29b and Σ45b, with a relative difference between 15 and 20 %. The nice agreement obtained between experimental and calculated values tends to confirm that the experimental GBs relative energies γ_s/γ_{gb} can be directly determined by applying the Mullins theory on the experimental ψ angles determined for all the GBs studied on our sample.

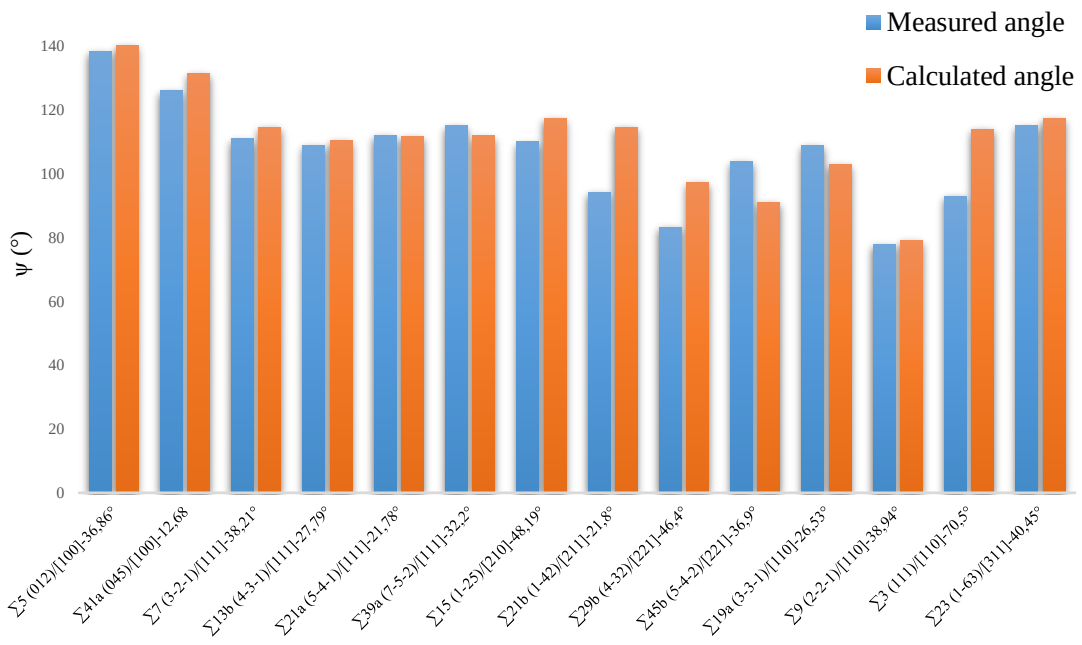

Figure 9: Comparison between the GB relative energies obtained from the experimental determination of dihedral angle at 1673 K (in blue) and from atomistic simulations at 1700 K (in orange).

Accordingly, the experimental dihedral angle ψ was used to determine the resulting GB relative energy by means of Herring equation. In Figure 10, γ_{gb}/γ_s values are plotted versus the misorientation angle θ for all investigated GBs at 1673 K. GBs possessing the same axis rotation are highlighted with the same color. γ_{gb}/γ_s ratio seems to be not correlated with the GB misorientation, and its values are found within the range 0.71 – 1.38, with the largest value for ∑9 corresponding to ψ = 78°.

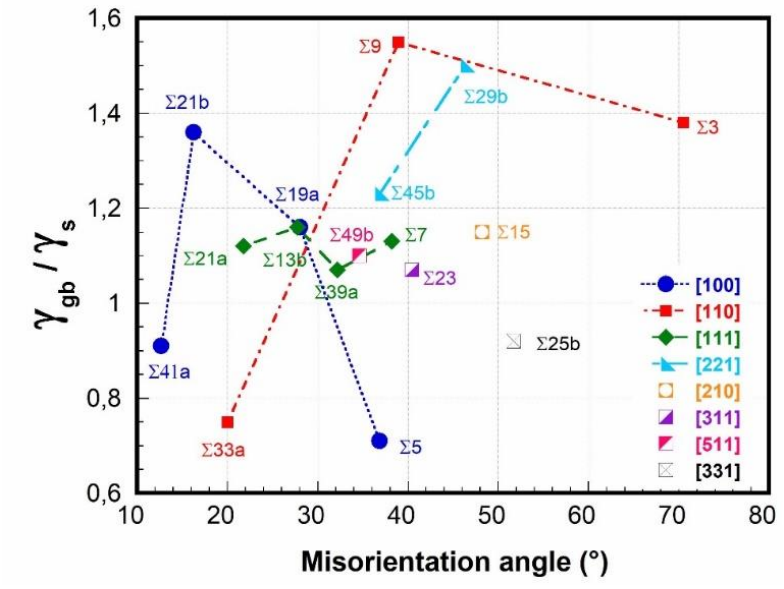

Figure 10 : GB relative energy as a function of misorientation angle at 1673 K.

Indeed, GBs having [100], [110] and [221] rotation axes display very distinct γ_{gb}/γ_s values and no trend behavior can be identified. However, GBs with a [111] rotation axis present similar γ_{gb}/γ_s values in a very closely range [1-1.2], suggesting that γ_{gb}/γ_s is insensitive to the misorientation angle in this case. $\sum$15, $\sum$23 and $\sum$49b present similar values compared to the latter. We note also that although $\sum$7 and $\sum$9 as well as $\sum$5 and $\sum$45b have nearly the same misorientation angle, they depict different γ_{gb}/γ_s values, and $\sum$19a and $\sum$13b display the same γ_{gb}/γ_s, whereas they present different $\sum$ values.

These results appear in agreement with several published studies [25,58] reporting that there is no simple relationship between the relative energy of a boundary and its macroscopic degrees of freedom, on the one hand, and that the crystallographic parameters such as a low value of $\sum$ were not necessarily indicative of a low energy, on the other hand. It is likely that the boundary energy is essentially related to the microscopic structure of the boundary with the atomic bonding playing a key role.

V. Conclusion

The dihedral angle ψ in UO_2 ceramics were assessed both experimentally and with atomistic simulations on CSL GBs. γ_{gb} of symmetric tilt GBs and γ_s of their respective boundary planes were calculated at 1700 K. The results support the idea that γ_S is identical at the groove of the GBs having the same rotation axis. Thus, the Herring equation could be useful for calculating the dihedral angle ψ.

In parallel, using EBSD-SEM and AFM techniques, faceted, asymmetrical and symmetrical grooves were evidenced on polycrystalline samples annealed at 1673 K for 4 h under Ar + 5% H_2 atmosphere. Thus, the GB dihedral angles were measured only on symmetrical grooves of a CSL GB. The comparison between measured and calculated ψ leads to an excellent agreement, suggesting that the Mullins theory can be used in UO_2 ceramics to experimentally determine the formation GBs energies by using identical γ_s at the root of the GB groove possessing the same rotation axis. This assumption is available only for GBs having similar γ_s values as a function of the rotation axis.

In summary, the marked agreement between the simulation and experimental approaches indicates that other key properties such as cleavage energies, which are very difficult to determine experimentally at the scale of the GBs, could be simulated as well. That would help providing a better understanding of the role of the GBs in the thermomechanical behavior of UO_2 ceramics under irradiation.

Acknowledgements

This work was granted access to the HPC resources of CINES and TGCC under the allocation 2018- A0030906922 made by GENCI.

References

[1] K.D. Reeve, Ceramics as nuclear reactor fuels, Ceramurg. Int. 1 (1975) 59–71. https://doi.org/10.1016/0390-5519(75)90008-3.

[2] P. Lejček, Grain Boundaries: Description, Structure and Thermodynamics, in: P. Lejcek (Ed.), Grain Bound. Segreg. Met., Springer Berlin Heidelberg, Berlin, Heidelberg, 2010: pp. 5–24. https://doi.org/10.1007/978-3-642-12505-8_2.

[3] L. Priester, Structures et défauts de structure des joints de grains, EDP Sciences, 2009. https://doi.org/10.1051/ptox/2009005.

[4] N.A. Gjostein, F.N. Rhines, Absolute interfacial energies of [001] tilt and twist grain boundaries in copper, Acta Metall. 7 (1959) 319–330. https://doi.org/10.1016/0001-6160(59)90198-1.

[5] G. Hasson, M. Biscondi, P. Lagarde, J. Levy, C. Goux, Structure of Grain Boundaries. Theoretical Determination and Experimental Observations, in: Nat. Behav. Grain Boundaries, Springer, Boston, MA, 1972: pp. 3–40. https://doi.org/10.1007/978-1-4757-0181-4_1.

[6] B.L. Adams, D. Kinderlehrer, W.W. Mullins, A.D. Rollett, S. Ta'asan, Extracting the relative grain boundary free energy and mobility functions from the geometry of microstructures, Scr. Mater. 38 (1998) 531–536. https://doi.org/10.1016/S1359-6462(97)00530-7.

[7] D.M. Saylor, A. Morawiec, G.S. Rohrer, The relative free energies of grain boundaries in magnesia as a function of five macroscopic parameters, Acta Mater. 51 (2003) 3675–3686. https://doi.org/10.1016/S1359-6454(03)00182-4.

[8] W. T. Read, W. Shockley, Dislocation Models of Crystal Grain Boundarm, Phys. Rev. 78 (1950) 275. https://doi.org/10.1103/PhysRev.78.275.

[9] C. Herring, Effect of Change of Scale on Sintering Phenomena, J. Appl. Phys. 21 (1950) 301–303. https://doi.org/10.1063/1.1699658.

[10] W.W. Mullins, Theory of Thermal Grooving, J. Appl. Phys. 28 (1957) 333–339. https://doi.org/10.1063/1.1722742.

[11] G. Dhalenne, A. Revcolevschi, A. Gervais, Grain boundaries in NiO. I. Relative energies of 〈001〉 tilt boundaries, Phys. Status Solidi A. 56 (1979) 267–276. https://doi.org/10.1002/pssa.2210560129.

[12] J.F. Shackelford, W.D. Scott, Relative Energies of Tilt Boundaries in Aluminum Oxide, J. Am. Ceram. Soc. 51 (1968) 688–692. https://doi.org/10.1111/j.1151-2916.1968.tb15929.x.

[13] R.L. Moment, R.B. Gordon, Energy of Grain Boundaries in Halite, J. Am. Ceram. Soc. 47 (1964) 570–573. https://doi.org/10.1111/j.1151-2916.1964.tb13819.x.

[14] A. Otsuki, Energies of (001) twist grain boundaries in silicon, Acta Mater. 49 (2001) 1737–1745. https://doi.org/10.1016/S1359-6454(01)00090-8.

[15] A. Otsuki, Variation of Energies of Aluminum [001] Boundaries with Misorientation and Inclination, Mater. Sci. Forum. 207–209 (1996) 413–416. https://doi.org/10.4028/www.scientific.net/MSF.207-209.413.

[16] A. Otsuki, H. Isono, M. Mizuno, ENERGY AND STRUCTURE OF [100] ALUMINIUM GRAIN BOUNDARY, J. Phys. Colloq. 49 (1988) C5-563-C5-568. https://doi.org/10.1051/jphyscol:1988569.

[17] C.A. Handwerker, J.M. Dynys, R.M. Cannon, R.L. Coble, Dihedral Angles in Magnesia and Alumina: Distributions from Surface Thermal Grooves, J. Am. Ceram. Soc. 73 (1990) 1371–1377. https://doi.org/10.1111/j.1151-2916.1990.tb05207.x.

[18] H. Yoshida, K. Yokoyama, N. Shibata, Y. Ikuhara, T. Sakuma, High-temperature grain boundary sliding behavior and grain boundary energy in cubic zirconia bicrystals, Acta Mater. 52 (2004) 2349–2357. https://doi.org/10.1016/j.actamat.2004.01.026.

[19] N. Shibata, F. Oba, T. Yamamoto, Y. Ikuhara §, Structure, energy and solute segregation behaviour of [110] symmetric tilt grain boundaries in yttria-stabilized cubic zirconia, Philos. Mag. 84 (2004) 2381–2415. https://doi.org/10.1080/14786430410001693463.

[20] M. Jin, S. Eriko, Y. Ikuma, Grain boundary grooving by surface diffusion in SrTiO3 bicrystal, J. Mater. Res. 14 (1999) 2548–2553. https://doi.org/10.1557/JMR.1999.0341.

[21] M.N. Kelly, S.A. Bojarski, G.S. Rohrer, The temperature dependence of the relative grain-boundary energy of yttria-doped alumina, J. Am. Ceram. Soc. 100 (2016) 783–791. https://doi.org/10.1111/jace.14488.
[22] D.M. Saylor, A. Morawiec, B.L. Adams, G.S. Rohrer, Misorientation Dependence of the Grain Boundary Energy in Magnesia, Interface Sci. 8 (2000) 131–140. https://doi.org/10.1023/A:1008764219575.
[23] S.J. Dillon, G.S. Rohrer, Characterization of the Grain-Boundary Character and Energy Distributions of Yttria Using Automated Serial Sectioning and EBSD in the FIB, J. Am. Ceram. Soc. 92 (2009) 1580–1585. https://doi.org/10.1111/j.1551-2916.2009.03064.x.
[24] N. Shibata, Y. Ikuhara, F. Oba, T. Yamamoto, T. Sakuma, Atomic structure and solute segregation of a Σ = 3, [110]/111 grain boundary in an yttria-stabilized cubic zirconia bicrystal, Philos. Mag. Lett. 82 (2002) 393–400. https://doi.org/10.1080/09500830210137407.
[25] E. Bourasseau, A. Mouret, P. Fantou, X. Iltis, R.C. Belin, Experimental and simulation study of grain boundaries in UO2, J. Nucl. Mater. 517 (2019) 286–295. https://doi.org/10.1016/j.jnucmat.2019.02.033.
[26] H. Ogawa, GBstudio: A Builder Software on Periodic Models of CSL Boundaries for Molecular Simulation, Mater. Trans. 47 (2006) 2706–2710. https://doi.org/10.2320/matertrans.47.2706.
[27] LAMMPS Documentation — LAMMPS documentation, (n.d.). https://lammps.sandia.gov/doc/Manual.html (accessed April 30, 2019).
[28] M.W.D. Cooper, M.J.D. Rushton, R.W. Grimes, A many-body potential approach to modelling the thermomechanical properties of actinide oxides, J. Phys. Condens. Matter. 26 (2014) 105401. https://doi.org/10.1088/0953-8984/26/10/105401.
[29] G. Gottstein, L.S. Shvindlerman, Grain boundary migration in metals : thermodynamics, kinetics, applications, Boca Raton ; London : CRC Press, 1999. https://trove.nla.gov.au/version/46594713 (accessed November 14, 2018).
[30] H. Matzke, T. Inoue, R. Warren, The surface energy of UO2 as determined by hertzian indentation, J. Nucl. Mater. 91 (1980) 205–220. https://doi.org/10.1016/0022-3115(80)90048-3.
[31] P.W. Tasker, The structure and properties of fluorite crystal surfaces, J. Phys. Colloq. 41 (1980) C6-488-C6-491. https://doi.org/10.1051/jphyscol:19806127.
[32] P. Nikolopoulos, S. Nazaré, F. Thümmler, Surface, grain boundary and interfacial energies in UO2 and UO2-Ni, J. Nucl. Mater. 71 (1977) 89–94. https://doi.org/10.1016/0022-3115(77)90191-X.
[33] E.N. Hodkin, M.G. Nicholas, Surface and interfacial properties of stoichiometric uranium dioxide, J. Nucl. Mater. 47 (1973) 23–30. https://doi.org/10.1016/0022-3115(73)90182-7.
[34] Y. Zhang, P.C. Millett, M.R. Tonks, X.-M. Bai, S.B. Biner, Molecular dynamics simulations of intergranular fracture in UO2 with nine empirical interatomic potentials, J. Nucl. Mater. 452 (2014) 296–303. https://doi.org/10.1016/j.jnucmat.2014.05.034.
[35] N.R. Williams, M. Molinari, S.C. Parker, M.T. Storr, Atomistic investigation of the structure and transport properties of tilt grain boundaries of UO2, J. Nucl. Mater. 458 (2015) 45–55. https://doi.org/10.1016/j.jnucmat.2014.11.120.
[36] A.S. Boyarchenkov, S.I. Potashnikov, K.A. Nekrasov, A.Y. Kupryazhkin, Molecular dynamics simulation of UO2 nanocrystals surface, J. Nucl. Mater. 421 (2012) 1–8. https://doi.org/10.1016/j.jnucmat.2011.11.030.
[37] G. Sattonnay, R. Tétot, Bulk, surface and point defect properties in UO2from a tight-binding variable-charge model, J. Phys. Condens. Matter. 25 (2013) 125403. https://doi.org/10.1088/0953-8984/25/12/125403.
[38] Necas, Klapetek, (PDF) Gwyddion: An open-source software for SPM data analysis, ResearchGate. (2011). https://doi.org/http://dx.doi.org/10.2478/s11534-011-0096-2.
[39] W.W. Mullins, Theory of linear facet growth during thermal etching, Philos. Mag. J. Theor. Exp. Appl. Phys. 6 (1961) 1313–1341. https://doi.org/10.1080/14786436108241227.

[40] J.R. Heffelfinger, C.B. Carter, Mechanisms of surface faceting and coarsening, Surf. Sci. 389 (1997) 188–200. https://doi.org/10.1016/S0039-6028(97)00411-1.
[41] D. Knoppik, H.-C. Bartscherer, {110} Surface structure and degree of coarsening of NaCl crystals annealed near the thermodynamic equilibrium of crystal and vapour, J. Cryst. Growth. 36 (1976) 342–344. https://doi.org/10.1016/0022-0248(76)90297-9.
[42] T.E. Madey, J. Guan, C.-H. Nien, C.-Z. Dong, H.-S. Tao, R.A. Campbell, FACETING INDUCED BY ULTRATHIN METAL FILMS ON W(111) AND Mo(111): STRUCTURE, REACTIVITY, AND ELECTRONIC PROPERTIES, Surf. Rev. Lett. 03 (1996) 1315–1328. https://doi.org/10.1142/S0218625X96002321.
[43] H. Matzke, C. Ronchi, Crystallographic shear and ordered reduction of UO2, Philos. Mag. J. Theor. Exp. Appl. Phys. 26 (1972) 1395–1407. https://doi.org/10.1080/14786437208220350.
[44] W. Zhang, P. Sachenko, I. Gladwell, Thermal grain boundary grooving with anisotropic surface free energies, Acta Mater. 52 (2004) 107–116. https://doi.org/10.1016/j.actamat.2003.08.033.
[45] P. Sachenko, J.H. Schneibel, W. Zhang, Effect of faceting on the thermal grain-boundary grooving of tungsten, Philos. Mag. A. 82 (2002) 815–829. https://doi.org/10.1080/01418610208243204.
[46] A. Szczepkowicz, R. Bryl, From hill-and-valley faceting to global faceting of a crystal: oxygen-covered tungsten, Surf. Sci. 559 (2004) L169–L172. https://doi.org/10.1016/j.susc.2004.04.035.
[47] Y. Miao, K. Mo, T. Yao, J. Lian, J. Fortner, L. Jamison, R. Xu, A.M. Yacout, Correlation between crystallographic orientation and surface faceting in UO2, J. Nucl. Mater. 478 (2016) 176–184. https://doi.org/10.1016/j.jnucmat.2016.05.044.
[48] H. Mykura, The variation of the surface tension of nickel with crystallographic orientation, Acta Metall. 9 (1961) 570–576. https://doi.org/10.1016/0001-6160(61)90160-2.
[49] K.-Y. Lee, E.D. Case, A comparison of theoretical and experimental profiles for thermally-induced grain-boundary grooving, Eur. Phys. J. - Appl. Phys. 8 (1999) 197–214. https://doi.org/10.1051/epjap:1999247.
[50] W. Shin, W.-S. Seo, K. Koumoto, Grain-boundary grooves and surface diffusion in polycrystalline alumina measured by atomic force microscope, J. Eur. Ceram. Soc. 18 (1998) 595–600. https://doi.org/10.1016/S0955-2219(97)00207-0.
[51] M.N. Kelly, W. Rheinheimer, M.J. Hoffmann, G.S. Rohrer, Anti-thermal grain growth in SrTiO3: Coupled reduction of the grain boundary energy and grain growth rate constant, Acta Mater. 149 (2018) 11–18. https://doi.org/10.1016/j.actamat.2018.02.030.
[52] D. Min, H. Wong, Grain-boundary grooving by surface diffusion with asymmetric and strongly anisotropic surface energies, J. Appl. Phys. 99 (2006) 023515. https://doi.org/10.1063/1.2159082.
[53] L. Klinger, E. Rabkin, Effects of Surface Anisotropy on Grain Boundary Grooving, Interface Sci. 9 (2001) 55–63. https://doi.org/10.1023/A:1011270830969.
[54] E. Rabkin, L. Klinger, V. Semenov, Grain boundary grooving at the singular surfaces, Acta Mater. 48 (2000) 1533–1540. https://doi.org/10.1016/S1359-6454(99)00432-2.
[55] L. Klinger, E. Rabkin, The effect of stress on grain boundary interdiffusion in a semi-infinite bicrystal, Acta Mater. 55 (2007) 4689–4698. https://doi.org/10.1016/j.actamat.2007.04.039.
[56] W. Zhang, P. Sachenko, J.H. Schneibel, Kinetics of Thermal Grain Boundary Grooving for Changing Dihedral Angles, J. Mater. Res. 17 (2002) 1495–1501. https://doi.org/10.1557/JMR.2002.0222.
[57] P.V. Nerikar, K. Rudman, T.G. Desai, D. Byler, C. Unal, K.J. McClellan, S.R. Phillpot, S.B. Sinnott, P. Peralta, B.P. Uberuaga, C.R. Stanek, Grain Boundaries in Uranium Dioxide: Scanning Electron Microscopy Experiments and Atomistic Simulations, J. Am. Ceram. Soc. 94 (2011) 1893–1900. https://doi.org/10.1111/j.1551-2916.2010.04295.x.
[58] A.P. Sutton, R.W. Balluffi, Overview no. 61 On geometric criteria for low interfacial energy, Acta Metall. 35 (1987) 2177–2201. https://doi.org/10.1016/0001-6160(87)90067-8.

***Declaration of Interest Statement**

Declaration of interests

☒ The authors declare that they have no known competing financial interests or personal relationships that could have appeared to influence the work reported in this paper.

☐The authors declare the following financial interests/personal relationships which may be considered as potential competing interests: